Free-standing P-doped Fe_2O_3/ZnO nanotubes as a bifunctional electrocatalyst for electrochemical water splitting

Pratap M. Ganje[1], Harshad A. Bandal*, Hern Kim*

Department of Energy Science and Technology, Environmental Waste Recycle Institute,

Myongji University, Yongin, Gyeonggi-do 17058, Republic of Korea
E-mail address: hernkim@mju.ac.kr (H. Kim)

Electronic Supporting Information

This electronic supplementary Information (ESI) shows the detailed explanation for preparation method of electrocatalyst and characterization methods.

SM.1 Preparation of RuO_2 electrode:

The RuO_2-supported nickel foam (NF) electrode was prepared using the standard drop casting process. The first back side of the NF (0.5 X 1.5 cm) was covered with epoxy glue to prevent the percolation of catalyst ink from the surface of NF and minimize the contribution of bare NF. The upper part of this NF was covered with epoxy glue in such a way that only (0.5 X 0.5 cm) area of NF was exposed with 10 µL catalyst ink consisting of 2.8 mg RuO_2, 10 µL Nafion (5 wt% in IPA), and 90 µL NMP dropped dried on the exposed surface of NF to afford an overall catalyst loading of ~1.1 mg cm^{-2}.

SM.2 Characterization of electrocatalyst:

XRD spectra were collected using a powder X-ray diffractometer (X pert MPD diffractometer) using CuKα radiation. The sample morphology was observed using a field-emission scanning electron microscope coupled with an energy dispersive X-ray spectrometer (FE-SEM-EDX, Hitachi S-3500 N, Japan) and transmission electron microscopy (TEM, Japan JEOL-3010)

equipped with EDS operated at an accelerating voltage of 300 kV. The Raman spectra were recorded using a high-resolution Raman spectrometer (Raman Spectroscope 8228). The Fe, P, Zn, and O element state was analyzed by X-ray photoelectron spectroscopy (XPS, Thermo Electron) using Mg Kα radiation.

SM.3 Double Layer Capacitance (DLC) measurement:

By using 1 M KOH electrolyte solution the electrochemical available surface area (ECSA) of all the electrocatalysts was derived from the double-layered capacitance (Cdl) values based on cyclic voltammetry. The electrocatalyst was covered with an epoxy glue limited area. The cyclic voltammograms were recorded in a non-Faradic region (-0.25 to -0.30 V vs. Hg/HgO) at various scan rates of 10, 20, 30, 40, and 50 mV/s. A linear trend has been seen when comparing the difference in current density (j) between the anodic and cathodic sweeps at 0.65 V vs. Hg/HgO against the scan rate. The slope of the line that fit was twice as steep as the Cdl.

SM.4 Estimation of electrochemical surface area:

Then, the electrochemical surface area (ECSA) has been calculated by following equation.

$$ECSA = {Cdl}/{Cs} \qquad (1)$$

The Cs is the specific capacitance, and the value of Cs is 0.04 mF cm^{-2} [1].

SM.5 Mott-Schottky calculation:

The flat band potential (V_{fb}) is calculated from the intercept of the MS plot on the X-axis while the Donor density (N_d) and Debye radius (L_D) were calculated using the following equations.

$$\frac{1}{C^2} = \frac{2}{eA^2 N_D \varepsilon \varepsilon_o}\left(V - V_{fb} - \frac{KT}{e}\right) \qquad (1)$$

$$N_D = \frac{2}{\varepsilon\varepsilon_\circ A^2 e \times Slope} \quad (2)$$

$$L_D = \sqrt{\left(\frac{\varepsilon\varepsilon_\circ KT}{2e^2 N_D}\right)} \quad (3)$$

$$V_{fb} = intercept - \left(\frac{KT}{e}\right) \quad (4)$$

Where, ε is the dielectric constant (12), ε_o is vacuum permittivity (8.854×10^{-12} F m^{-1}), A is the BET surface area (Fig. S18), and K is the Boltzmann constant, and T is the temperature (298 ^{O} kelvin), e is the electronic charge (1.602×10^{-19} coulombs).

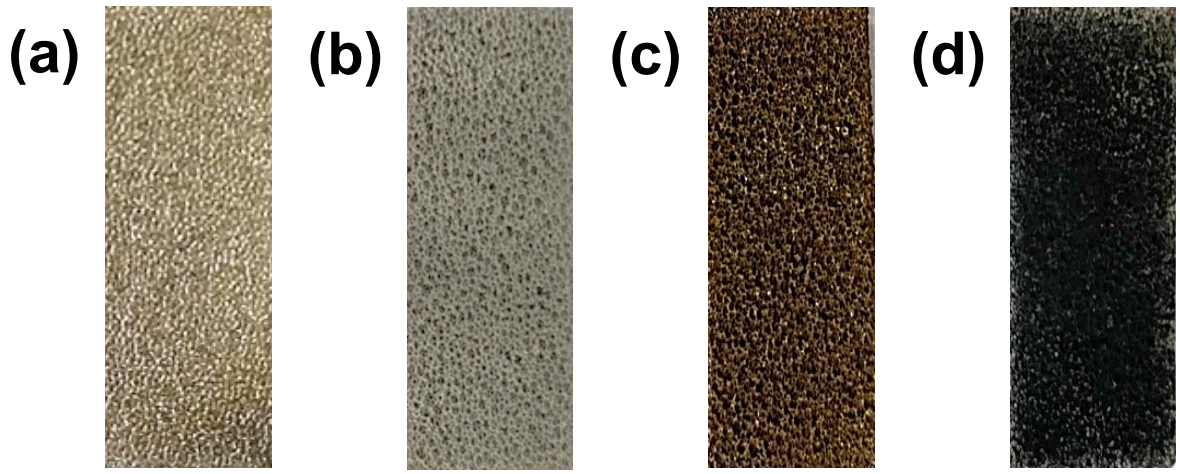

Fig S 1 photographs of (a) nickel foam, (b) ZnO treatment, (c) Fe ZnO, (d) FO-P2

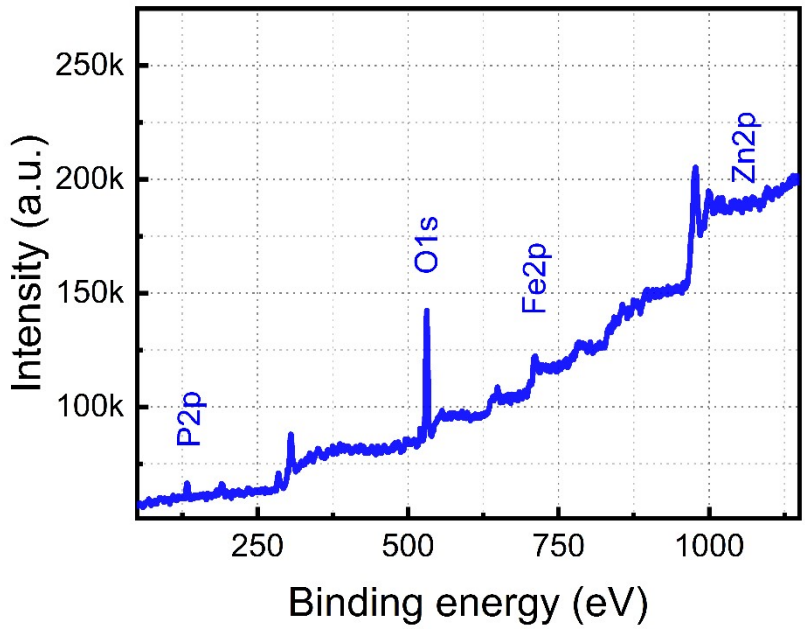

Fig S 2 XPS survey spectra of FO-P2

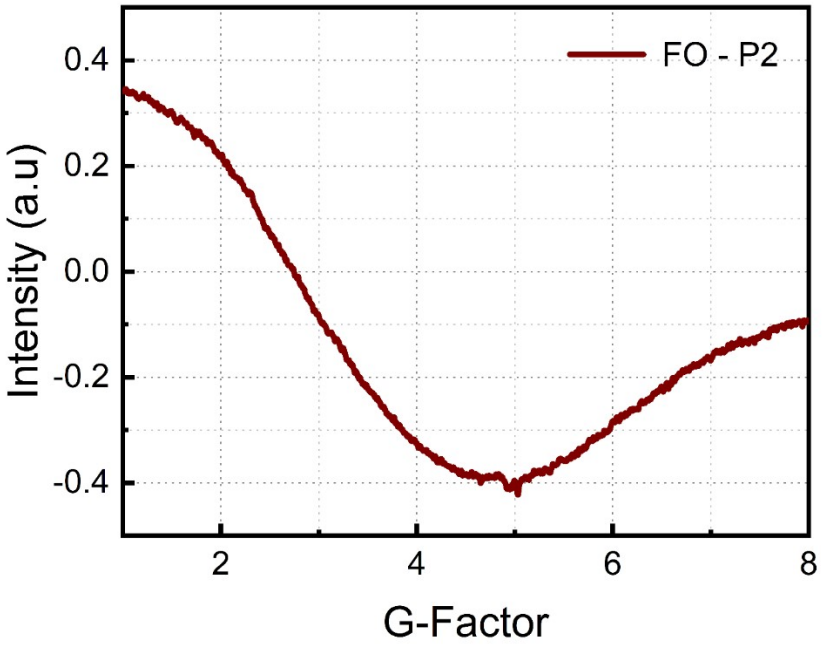

Fig S 3 EPR spectra of FO-P2

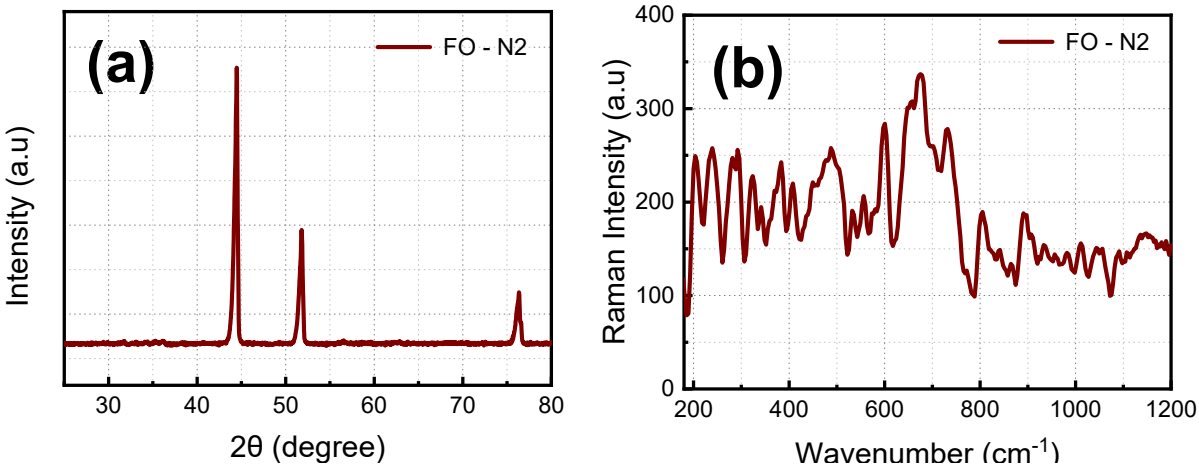

Fig S 4 (a) X-ray diffraction spectra of FO-N2, (b) Raman spectra of FO-N2

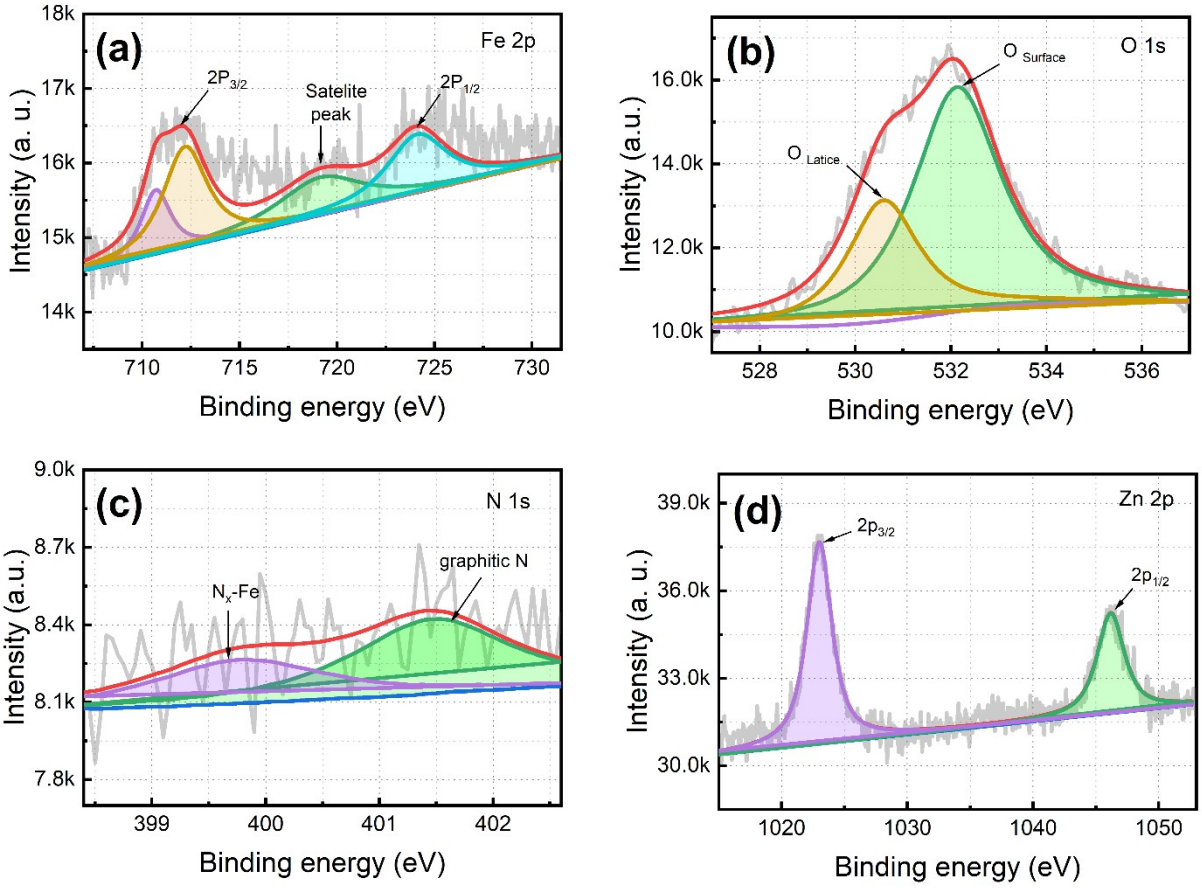

Fig S 5 XPS analysis of FO-N2; (a) High resolution Fe 2p spectra, (b) High resolution O 1s spectra (c) High resolution N 1s spectra, (d) High resolution Zn 2p spectra.

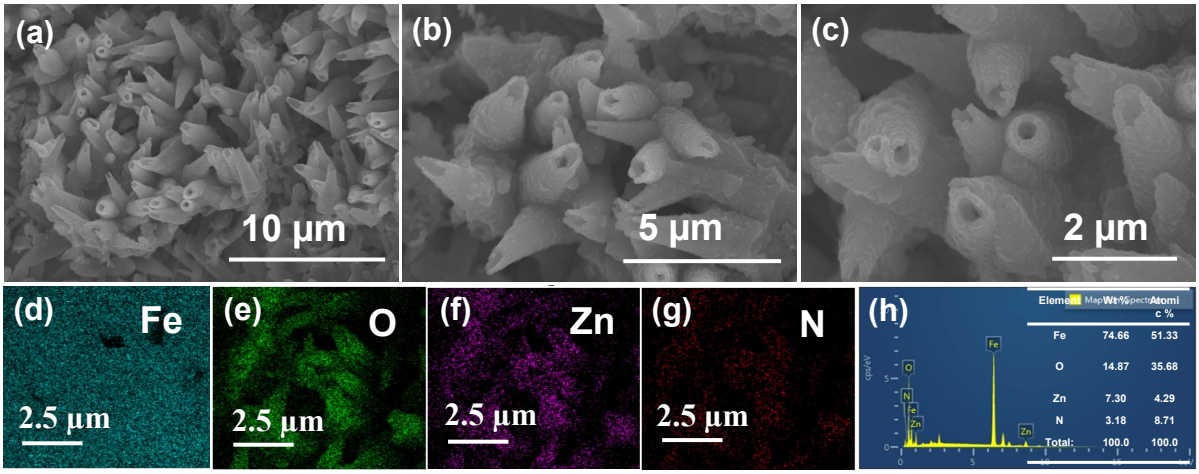

Fig S 6 SEM image of FO-N2 (a-c), elemental mapping of Fe, O, Zn, N elements (d-g), EDX Mapping of elements

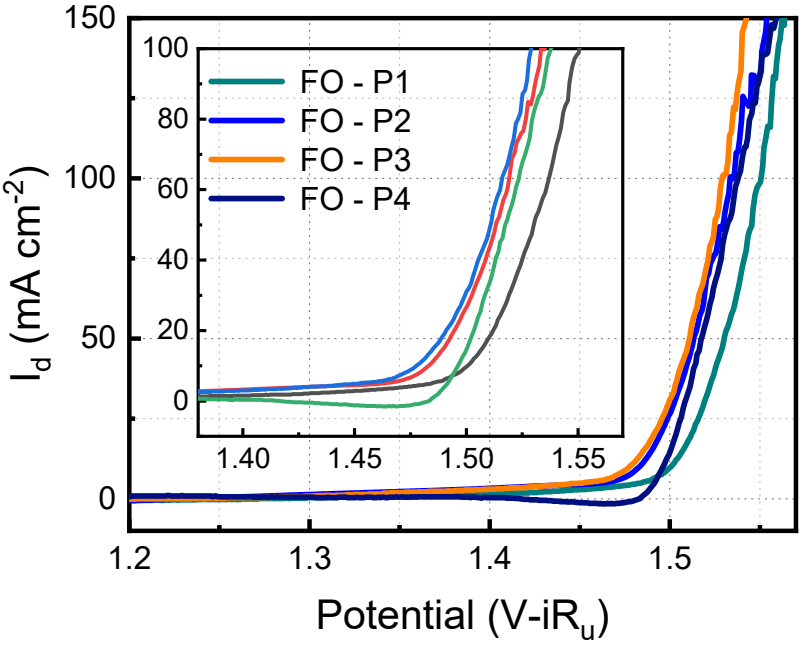

Fig S 7 LSV of samples collected after different phosphorization time

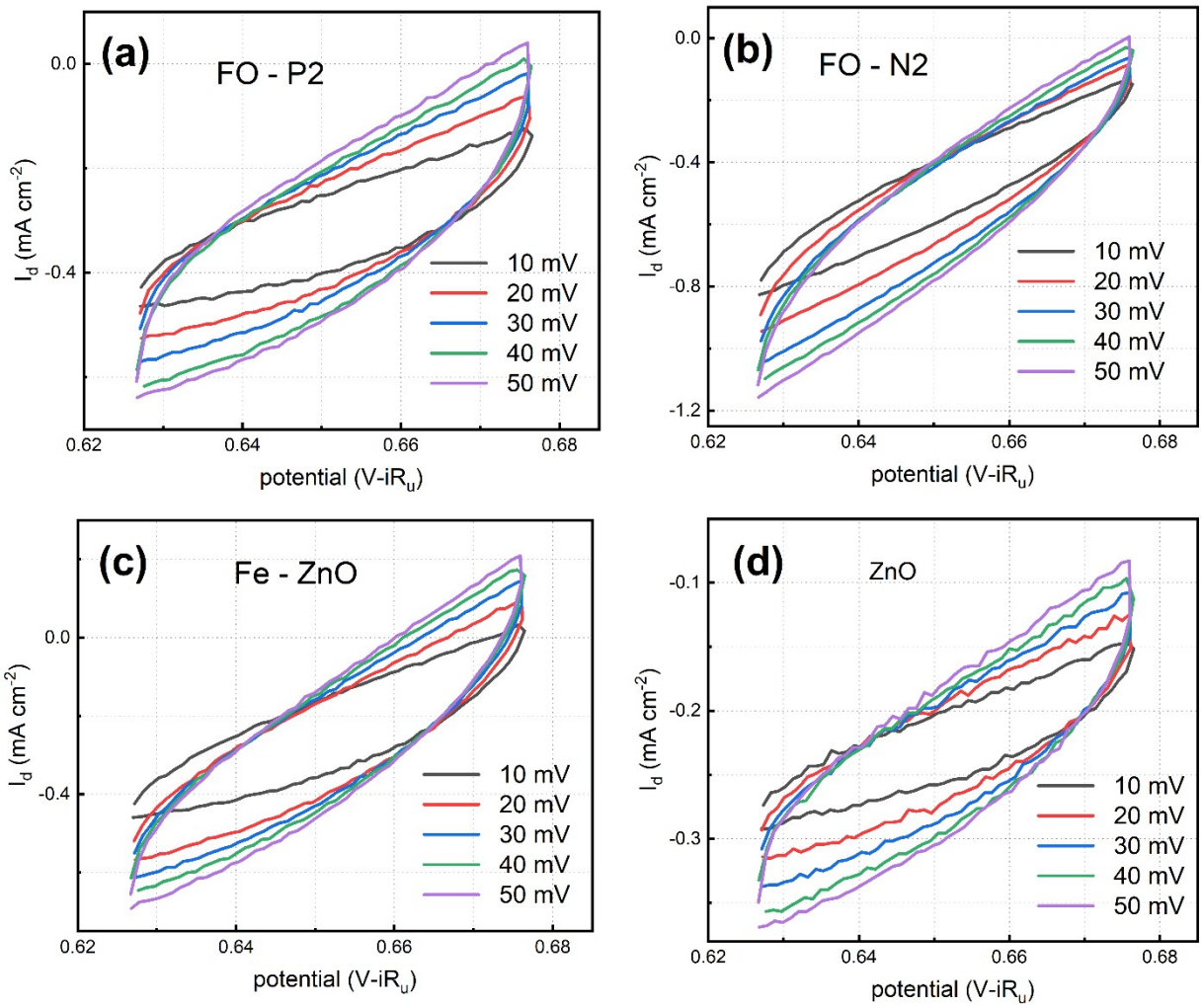

Fig S 8 CV curve collected for the measurement of DLC of different catalyst (a) FO-P2, (b) FO-N2, (C) Fe-ZnO, (d) ZnO

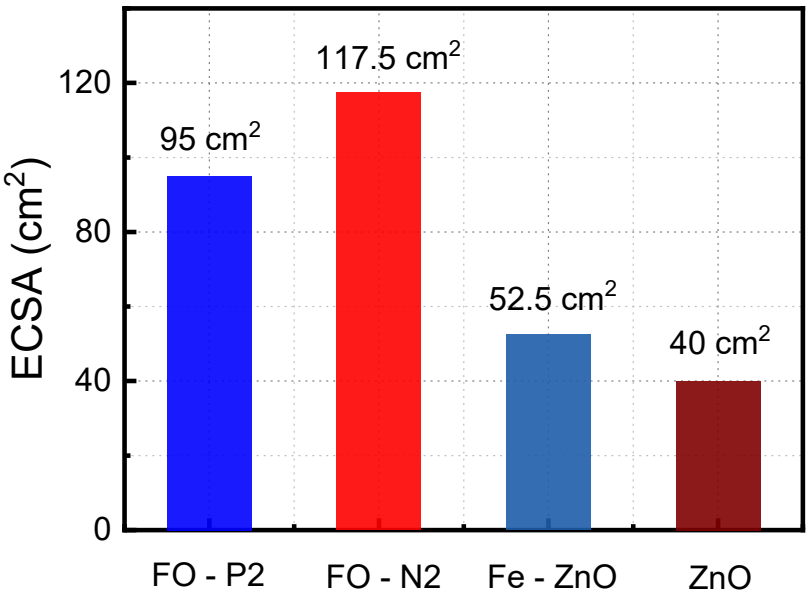

Fig S 9 ECSA of different catalyst

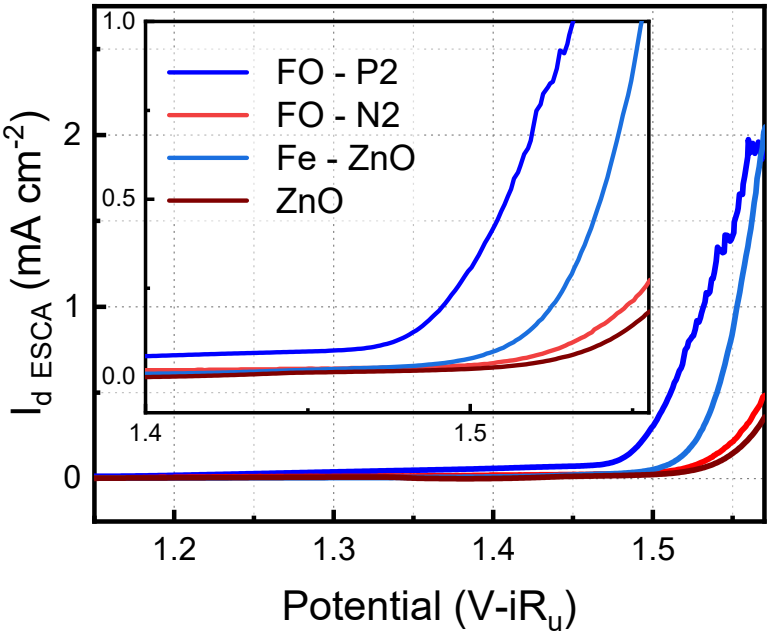

Fig S 10 LSV curve of different catalysts normalized with respect to ECSA

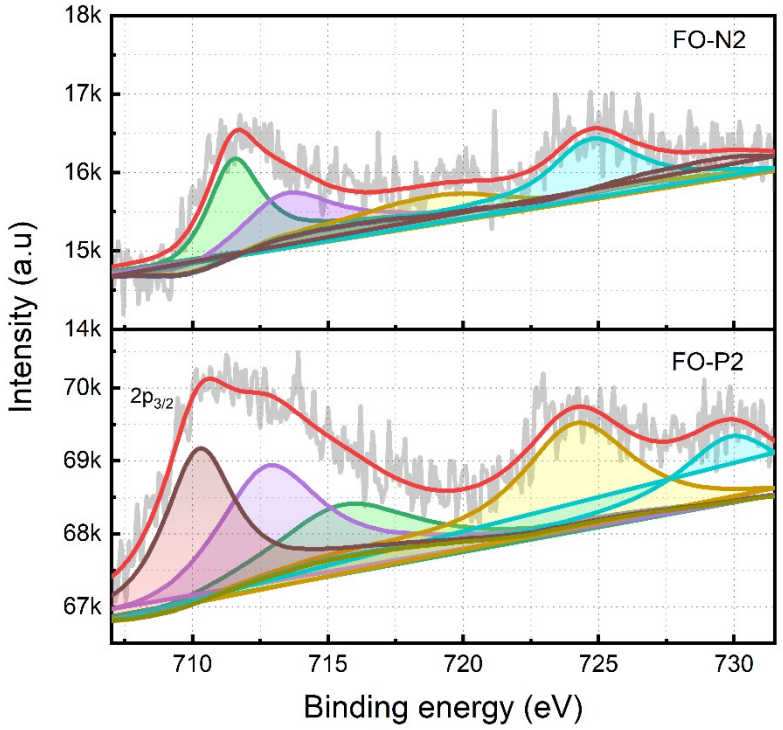

Fig S 11 Comparison between Fe2p region of XPS spectra of FO-P2 and FO-N2

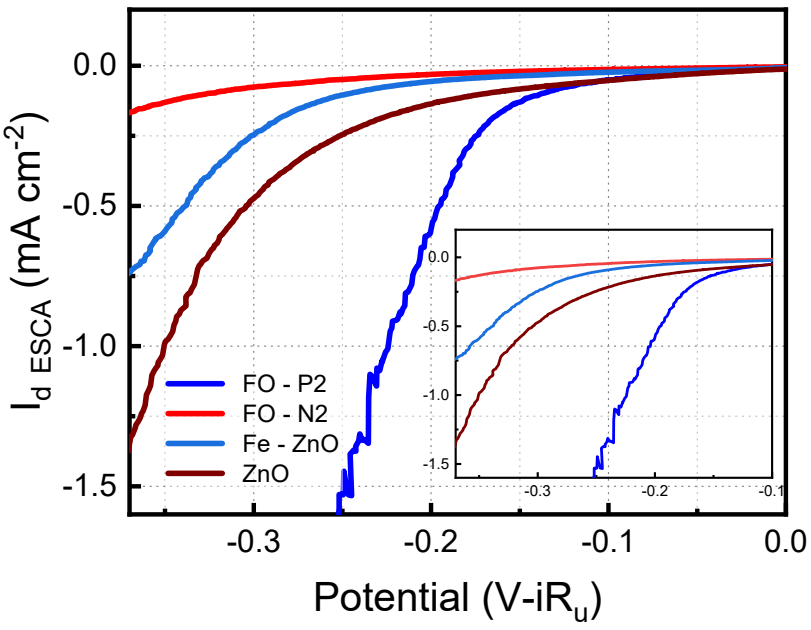

Fig S 12 LSV curve normalized with respect to ECSA

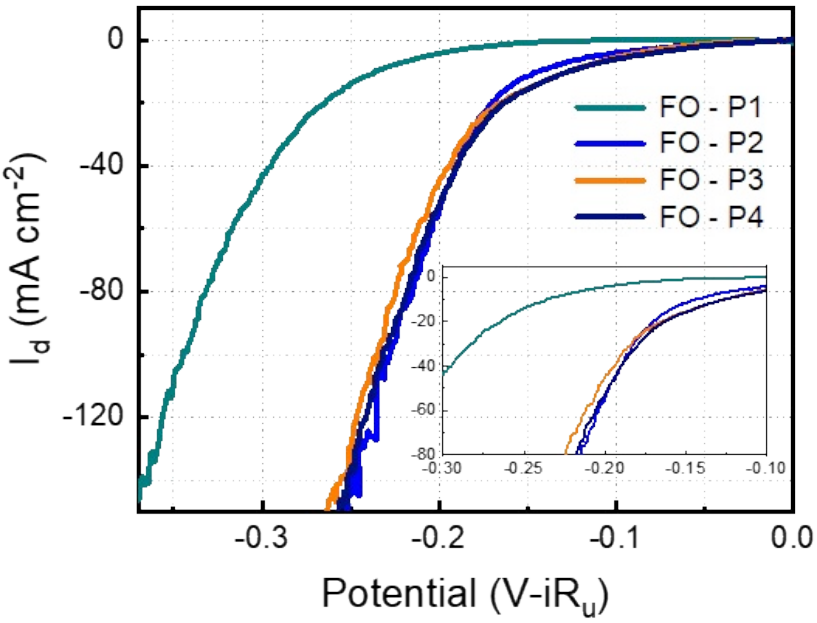

Fig S 13 Dependence of HER activity on phosphorization time

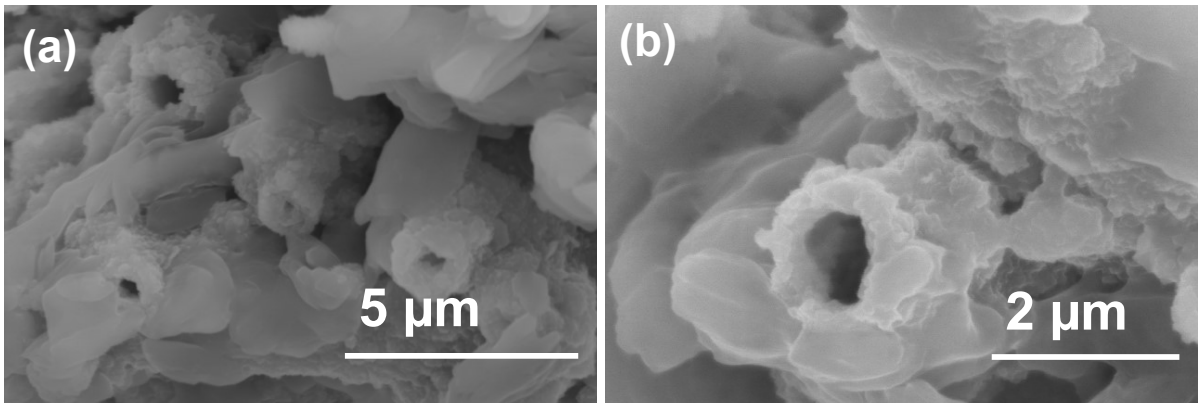

Fig S 14 SEM image of FO-P2 collected after HER

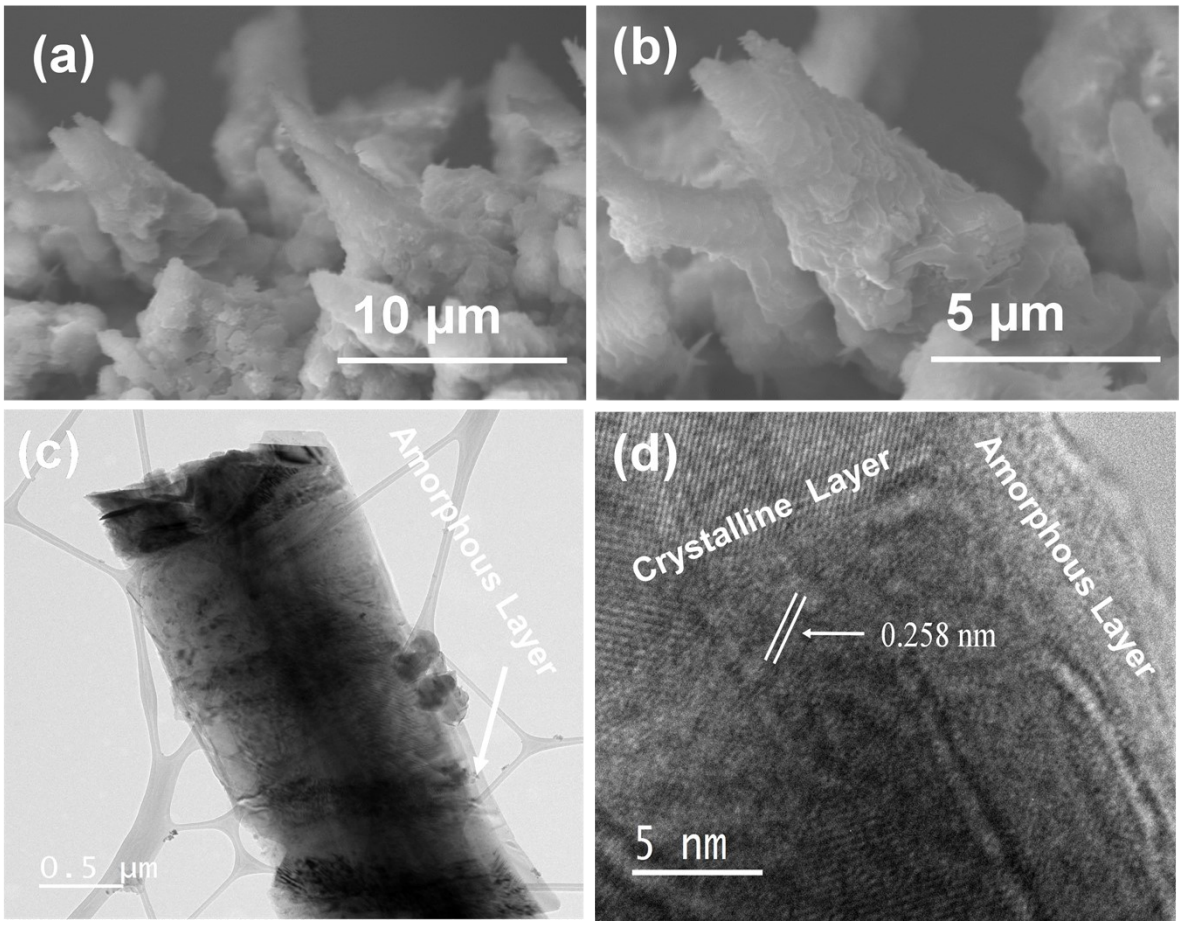

Fig S 15 (a,b) SEM images of FO-P2 after OER, (c, d) TEM images of FO-P2 after OER

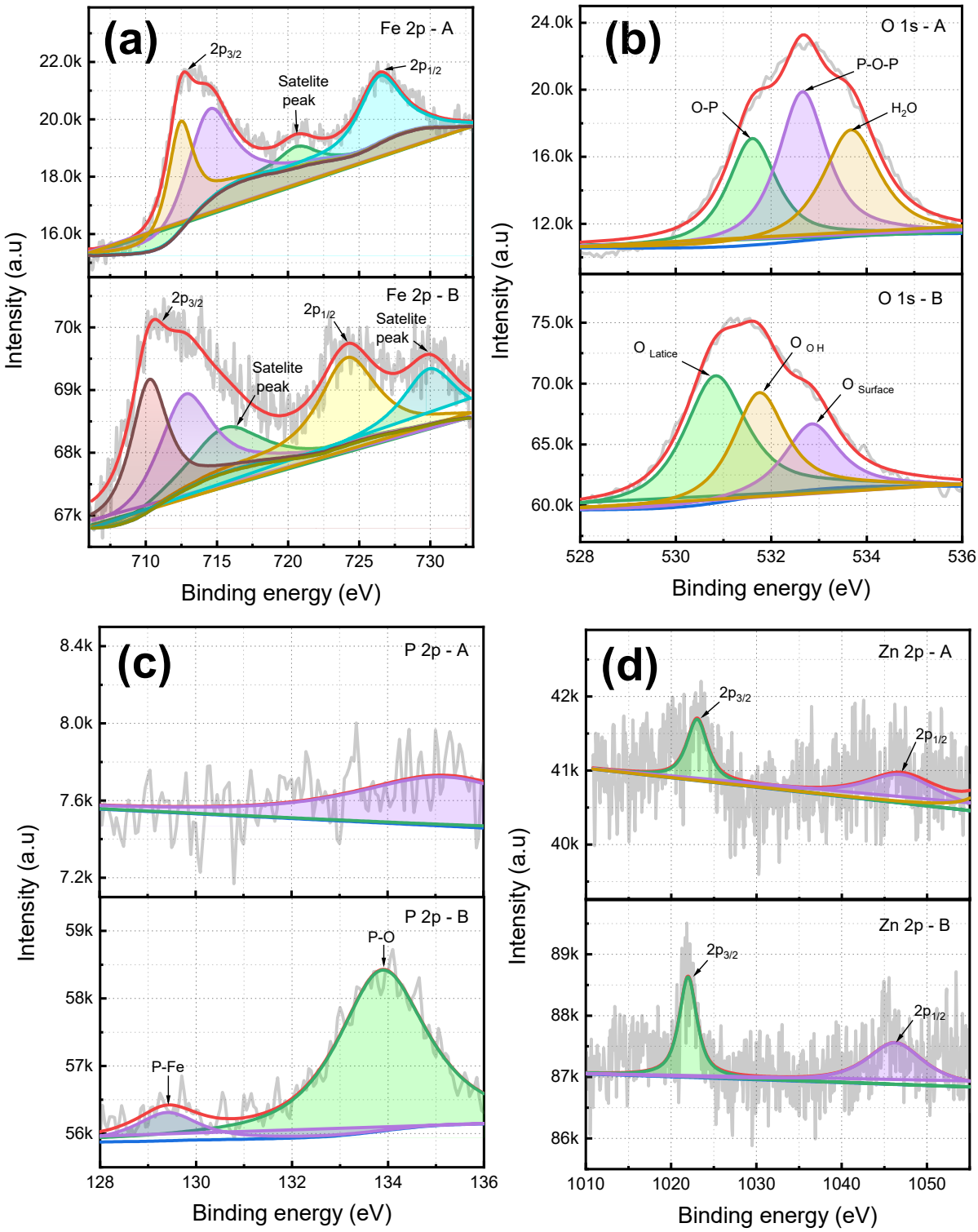

Fig S 16 XPS analysis of FO-P2 (comparison between before and after water splitting reaction); (a) High resolution Fe 2p spectra, (b) High resolution O 1s spectra (c) High resolution P 2p spectra, (d) High resolution Zn 2p spectra.

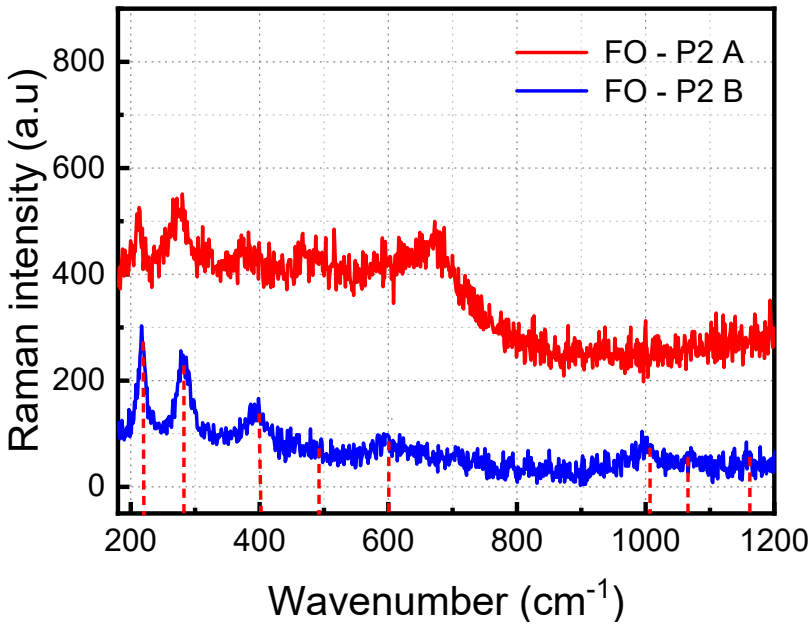

Fig S 17 Raman spectra of FO-P2 collected before and after OER

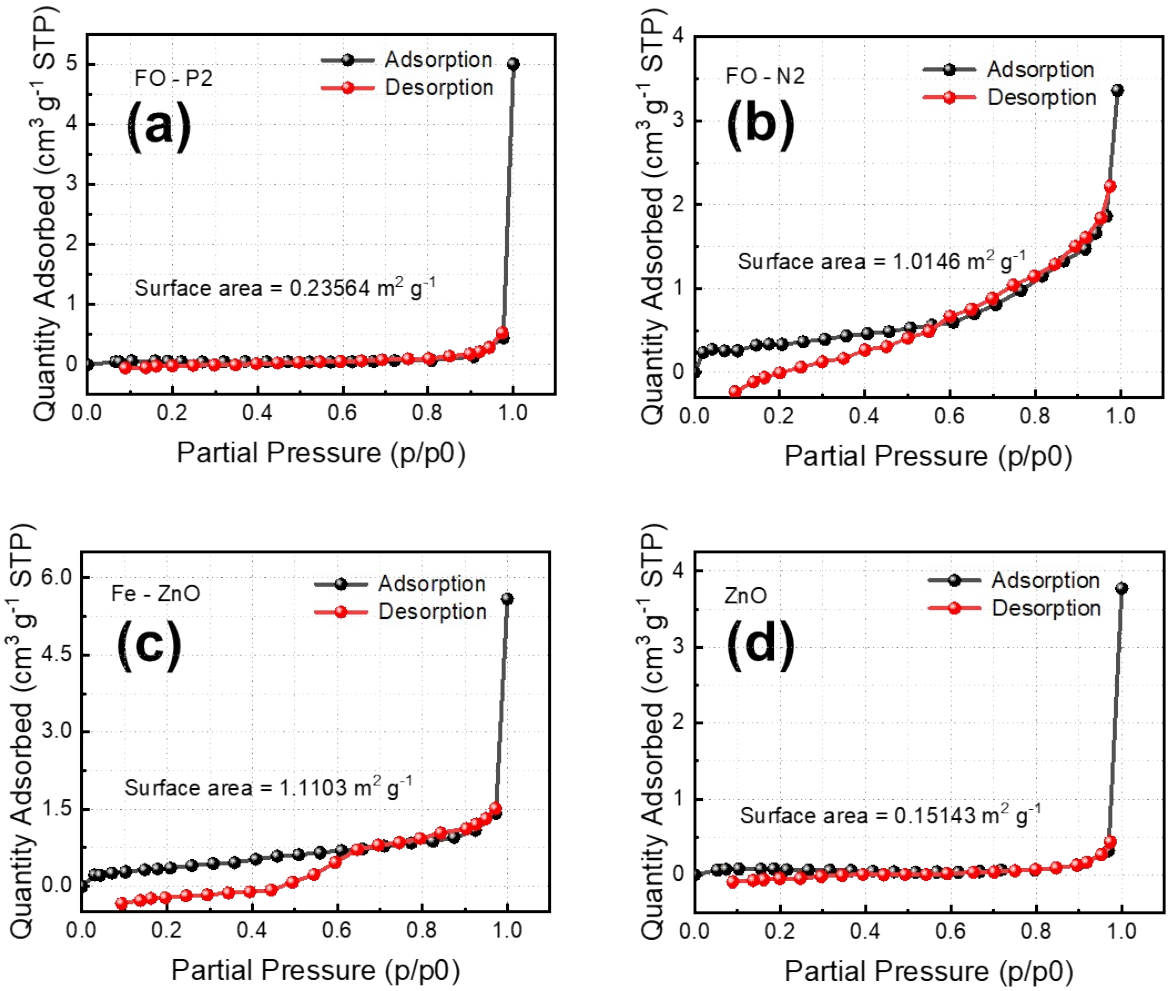

Fig S 18 BET surface area analysis of different catalysts (a) FO-P2, (b) FO-N2, (c) Fe-ZnO, (d) ZnO

Table. S1 Performance comparison of FO-P2 with other reported materials in previous literature towards OER application.

Sr. No	Electrocatalyst	Electrolyte OER	η value at 10 mA cm^{-2}	Tafel slope mV/dec^{-2}	Reference
1	P-Fe_2O_3-$_{0.45}$	1 M KOH	270 mV	72.1	[3]
2	P-Co_3O_4	1 M KOH	280 mV	51.6	[4]
3	Fe-P@CP	1 M KOH	290 mV	63.6	[5]
4	ZnO/FeOOH/NF	1 M KOH	301 mV	50.0	[6]
5	Fe CoO-NF	1 M KOH	244 mV	57.0	[7]
6	Ni CoFeP/C	1 M KOH	270 mV	65.0	[8]
7	Fe_2O_3/CNT	1 M KOH	383 mV	68.0	[9]
8	FeP-FePxOy	1 M KOH	280 mV	48.0	[10]
9	Fe-NiO-Ni	1 M KOH	245 mV	43.4	[11]
10	FO $_{800}$	1 M KOH	330 mv	52	[12]
11	Co $_{0.20}$ Fe $_{0.80}$ OOH	1 M KOH	383 mv	40	[13]
12	α-Fe_2O_3	1 M KOH	317 mv	58.5	[14]
13	Fe/Fe3C–F@CNT	1 M KOH	286 mv	49	[15]
14	c-Fe_2O_3	1 M KOH	650 mv	56	[16]
15	Hm	1 M KOH	280 mv	43	[17]
16	CoPO/NF	1 M KOH	116 mV	65.6	[18]
17	Fe1Co1-ONS	1 M KOH	350 mV	36.8	[19]
18	FO - N2	1 M KOH	299 mV	61.0	This work
19	FO – P2	1 M KOH	240 mV	40.0	This work

Table. S2 Value of different parameters obtained by fitting EIS data in an equivalent circuit.

Electrodes	FO - P2	FO - N2	Fe - ZnO	ZnO
R_S (ohm)	2.96	2.227	2.339	2.203
R_1 (ohm)	6.176	73.933	86.66	185.102
Qy_1 (S s^n cm^{-2})	0.18429	0.004958	0.019185	0.009141
Qa_1	0.30338	0.685676	0.609204	0.649575
R_2 (ohm)	3.828	30.964	6.747	34.1
Qy_2 (S s^n cm^{-2})	0.02145	0.017521	0.009962	0.004496
Qa_2	0.86911	0.996524	1.025	0.775505

Catalyst	Slope	N_D	L_D	V_{fb}
FO-P2	16.77585	7.88396 X 10^{23}	3.2867E-09	0.250177515
FO-N2	71.2438	1.00136E+22	2.91634E-08	0.281897515
Fe-ZnO	64.01017	9.30673E+21	3.02506E-08	0.292807515

Table. S3 Values of different parameters obtained MS analysis.

Table. S4 Performance comparison of FO-P2 with other reported materials in previous literature towards HER application.

Sr. No	Electrocatalyst	Electrolyte HER	η value at 10 mA cm^{-2}	Tafel slope mV/dec^{-2}	Reference
1	P-Co_3O_4	1 M KOH	120 mV	52.0	[4]
2	Fe-P/Ti	1 M KOH	95 mV	-	[20]
3	Fe-P	1 M KOH	194 mV	75.0	[21]
4	Fe CoO-NF	1 M KOH	205 mV	118.0	[7]
5	Ni CoFeP/C	1 M KOH	149 mV	89.0	[8]
6	Ni-Fe_2O_3	1 M KOH	310 mV		[22]
7	Ni-FeP/C	1 M KOH	95 mV	72	[23]
8	N-FeP	1 M KOH	226 mV	84.8	[24]
9	NiCoFeP	1 M KOH	131 mV	56	[25]
10	Mn-FeP	1 M KOH	173 mV	95	[26]
11	Vc-FeP	1 M KOH	108 mV	62	[27]
12	Ni-Fe-P	1 M KOH	142 mV	84.24	[28]
13	Ni-Fe/NF	1 M KOH	142 mV	133.3	[29]
14	Co-Fe-P	1 M KOH	73 mV	44	[30]
15	$Co_{0.75}Fe_{0.25}$-NC	1 M KOH	202 mV	67.96	[31]
16	$Co_{0.59}Fe_{0.41}P$	1 M KOH	92 mV	72	[32]
17	Ni_2P nanosheets	1 M KOH	168 mV	63	[13]
18	Fe^{3+}Ni@NCF	1 M KOH	219 mV	109.9	[33]
19	FO - N2	1 M KOH	312 mV	315	This work
20	FO – P2	1 M KOH	139 mV	104	This work

Reference:

1 C. C. L. McCrory, S. Jung, J. C. Peters and T. F. Jaramillo, *J. Am. Chem. Soc.*, 2013, **135**, 16977–16987.

2 A. Banerjee, V. Aravindan, S. Bhatnagar, D. Mhamane, S. Madhavi and S. Ogale, *Nano Energy*, 2013, **2**, 890–896.

3 Y. L. Tong, B. Q. Chi, D. L. Qi and W. Zhang, *RSC Adv.*, 2021, **11**, 1233–1240.

4 Z. Xiao, Y. Wang, Y.-C. Huang, Z. Wei, C.-L. Dong, J. Ma, S. Shen, Y. Li and S. Wang, *Energy Environ. Sci.*, 2017, **10**, 2563–2569.

5 D. Xiong, X. Wang, W. Li and L. Liu, *Chem. Commun.*, 2016, **52**, 8711–8714.

6 L. Zhang, H. Li, B. Yang, N. Han, Y. Wang, Z. Zhang, Y. Zhou, D. Chen and Y. Gao, *J. Solid State Electrochem.*, 2020, **24**, 905–914.

7 H. A. Bandal, A. R. Jadhav, A. H. Tamboli and H. Kim, *Electrochim. Acta*, 2017, **249**, 253–262.

8 X. Wei, Y. Zhang, H. He, L. Peng, S. Xiao, S. Yao and P. Xiao, *Chem. Commun.*, 2019, **55**, 10896–10899.

9 H. A. Bandal, A. R. Jadhav, A. A. Chaugule, W. J. Chung and H. Kim, *Electrochim. Acta*, 2016, **222**, 1316–1325.

10 J. Xu, D. Xiong, I. Amorim and L. Liu, *ACS Appl. Nano Mater.*, 2018, **1**, 617–624.

11 Y. Lei, T. Xu, S. Ye, L. Zheng, P. Liao, W. Xiong, J. Hu, Y. Wang, J. Wang, X. Ren, C.

He, Q. Zhang, J. Liu and X. Sun, *Appl. Catal. B Environ.*, 2021, **285**, 119809.

12 H. A. Bandal, A. A. Pawar and H. Kim, *Electrochim. Acta*, 2022, **422**, 140545.

13 D. Inohara, H. Maruyama, Y. Kakihara, H. Kurokawa and M. Nakayama, *ACS Omega*, 2018, **3**, 7840–7845.

14 H. Wu, T. Yang, Y. Du, L. Shen and G. W. Ho, *Adv. Mater.*, 2018, **30**, 1–9.

15 T. Gao, C. Zhou, Y. Zhang, Z. Jin, H. Yuan and D. Xiao, *J. Mater. Chem. A*, 2018, **6**, 21577–21584.

16 W. L. Kwong, C. C. Lee, A. Shchukarev, E. Björn and J. Messinger, *J. Catal.*, 2018, **365**, 29–35.

17 B. Mohanty, Y. Wei, M. Ghorbani-Asl, A. V. Krasheninnikov, P. Rajput and B. K. Jena, *J. Mater. Chem. A*, 2020, **8**, 6709–6716.

18 Y. Liu, D. Yang, Z. Liu and J. H. Yang, *J. Power Sources*, 2020, **461**, 228165.

19 L. Zhuang, L. Ge, Y. Yang, M. Li, Y. Jia, X. Yao and Z. Zhu, *Adv. Mater.*, 2017, **29**, 1606793.

20 X. Zhao, Z. Zhang, X. Cao, J. Hu, X. Wu, A. Y. R. Ng, G. P. Lu and Z. Chen, *Appl. Catal. B Environ.*, 2020, **260**, 118156.

21 C. Y. Son, I. H. Kwak, Y. R. Lim and J. Park, *Chem. Commun.*, 2016, **52**, 2819–2822.

22 L. Zeng, K. Zhou, L. Yang, G. Du, L. Liu and W. Zhou, *ACS Appl. Energy Mater.*, 2018, **1**, 6279–6287.

23 S. Xu, H. Zhao, T. Li, J. Liang, S. Lu, G. Chen, S. Gao, A. M. Asiri, Q. Wu and X. Sun,

J. Mater. Chem. A, 2020, **8**, 19729–19745.

24 J. Huang, J. Han, T. Wu, K. Feng, T. Yao, X. Wang, S. Liu, J. Zhong, Z. Zhang, Y. Zhang and B. Song, *ACS Energy Lett.*, 2019, 3002–3010.

25 Z. Ge, B. Fu, J. Zhao, X. Li, B. Ma and Y. Chen, *J. Mater. Sci.*, 2020, **55**, 14081–14104.

26 M. Wang, Y. Tuo, X. Li, Q. Hua, F. Du and L. Jiang, *ACS Sustain. Chem. Eng.*, 2019, **7**, 12419–12427.

27 J. Duan, S. Chen, C. A. Ortíz-Ledón, M. Jaroniec and S. Qiao, *Angew. Chem. Int. Ed. Engl.*, 2020, **59**, 8181–8186.

28 Z. Ma, R. Li, M. Wang, H. Meng, F. Zhang, X. Q. Bao, B. Tang and X. Wang, *Electrochim. Acta*, 2016, **219**, 194–203.

29 Z. Zhang, Y. Wu and D. Zhang, *Int. J. Hydrogen Energy*, 2022, **47**, 1425–1434.

30 H. Kim, S. Oh, E. Cho and H. Kwon, *ACS Sustain. Chem. Eng.*, 2018, **6**, 6305–6311.

31 X. Feng, X. Bo and L. Guo, *J. Power Sources*, 2018, **389**, 249–259.

32 X. Wen and J. Guan, *Appl. Mater. Today*, 2019, **16**, 146–168.

33 Z. Zhang, L. Cong, Z. Yu, L. Qu and W. Huang, *Mater. Today Energy*, 2020, **16**, 100387.